

# Dense, Self-Formed Char Layer Enables a Fire-Retardant Wood Structural Material

Wentao Gan, Chaoji Chen, Zhengyang Wang, Jianwei Song, Yudi Kuang, Shuaiming He, Ruiyu Mi, Peter B. Sunderland, and Liangbing Hu\*

Wood is one of the most abundant, sustainable, and aesthetically pleasing structural materials and is commonly used in building and furniture construction. Unfortunately, the fire hazard of wood is a major safety concern for its practical applications. Herein, an effective and environmentally friendly method is demonstrated to substantially improve the fire-retardant properties of wood materials by delignification and densification. The densification process eliminates the spaces between the cell walls, leading to a highly compact laminated structure that can block oxygen from infiltrating the material. In addition, an insulating wood char layer self-formed during the burning process obstructs the transport of heat and oxygen diffusion. These synergistic effects contribute to the material's excellent fire-retardant and self-extinguished properties, including a 2.08-fold enhancement in ignition time ( $t_{ig}$ ) and 34.6% decrease in maximum heat release rate. Meanwhile, the densified wood shows a more than 82-fold enhancement in compressive strength compared with natural wood after exposure to flame for 90 s, which could effectively prevent the collapse and destruction of wooden structures, and gain precious rescue time when a fire occurs. The facile top-down chemical delignification and densification process enabling both substantially enhances fire-retardant performance and mechanical robustness represents a promising direction toward fire-retardant and high-strength structural materials.

## 1. Introduction

In the United States, there were more than 1.3 million fires in 2016 alone, leading to an estimated 3390 civilian deaths, which represents the highest number of fatalities since 2008.<sup>[1]</sup> The flammability of wooden homes and furniture has been cited as mainly responsible for these injuries. Wood is one of the oldest

building materials and commonly used in construction, furniture, and decoration because of its lightweight, mechanical robustness, texture, and thermal and electrical insulating properties.<sup>[2–6]</sup> Fire safety, however, represents a major restriction for wood materials when used in structural applications. Impregnating halogenated flame retardants into wood pores through physical infiltration is a traditional flame-retardant treatment; however, these compounds do not meet the high environmental and health requirements for modern buildings due to the risk of bioaccumulation in people.<sup>[7,8]</sup>


Recently, the development of nanotechnologies and bionic design has enabled efficient solutions for the fire retardancy of engineering materials, especially wood, in a more environmentally friendly way.<sup>[9–14]</sup> For example, hybridizing wood with inorganic nanoparticles made of clay, Mg–Al-layered double-hydroxide, and calcium carbonate has proven effective at forming functional inorganic/organic materials with good thermal resistance and fire retardancy.<sup>[15–18]</sup> However, nanoparticle coatings may be too expensive for commercial use, as well as

demonstrating unsatisfactory structural strength and stability. In addition, the rapid destruction and collapse of wooden buildings are other main causes of fire damage, highlighting the importance of combining both fire retardancy and mechanical robustness in a single material.

Herein, we develop a delignification-assisted densification strategy to simultaneously enhance the mechanical robustness and flame-retardant properties of wood materials with oriented cellulose nanofibrils in an environmentally friendly, low-cost, and scalable way. The delignification and densification process via mechanical pressing can completely remove the spaces between the wood cell walls, leading to a highly dense laminated structure (Figure 1a). Such a dense laminated structure not only effectively reduces the air permeability (Figure S1, Supporting Information) of the material, but also conduces the formation of an insulating char layer on the wood surface should the material catch fire (Figure 1b). The dense wood char layer creates an insulating barrier to the underlying wood, resulting in improved fire retardance by reducing both the thermal and oxygen diffusion, which plays a vital role in

W. Gan, Dr. C. Chen, Dr. J. Song, Y. Kuang, S. He, R. Mi, Prof. L. Hu  
Department of Materials Science and Engineering  
University of Maryland  
College Park, MD 20742, USA  
E-mail: binghu@umd.edu

Z. Wang, Prof. P. B. Sunderland  
Department of Fire Protection Engineering  
University of Maryland  
College Park, MD 20742, USA

 The ORCID identification number(s) for the author(s) of this article can be found under <https://doi.org/10.1002/adfm.201807444>.

DOI: 10.1002/adfm.201807444

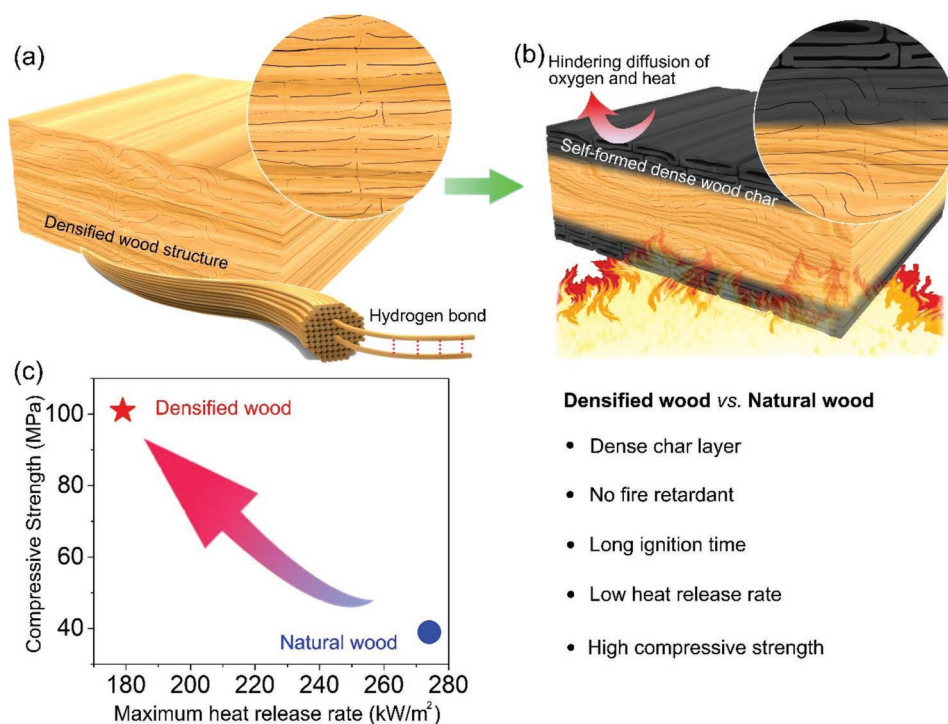


**Figure 1.** Schematic representation demonstrating the working principle of the self-formed wood char layer of densified wood for fire resistance. a) The densified structure of the wood with oriented cellulose nanofibrils limits the amount of oxygen inside the material. b) Upon catching fire, the wood char formed on the outside of the densified wood plays a role in protecting the internal wood structure. c) The compressive strength of densified wood is shown to be significantly higher than natural wood, and the maximum heat release rate of the densified wood at an external heat flux of 30 kW m<sup>-2</sup> is shown to be significantly lower than natural wood, demonstrating its great mechanical property and excellent fire retardance.

reducing the heat release rate (HRR), hindering the combustion reaction (Figure 1c). In addition to good fire retardance, the densified wood also possesses excellent compressive strength, which effectively prevents the collapse and destruction of the wooden structure, gaining precious rescue time should a fire occur (Figure 1c). The fire retardant and strong wood achieved without the use of halogenated chemicals or nanomaterial coatings demonstrates both efficient fire-retardant performance and excellent mechanical properties, with strong potential for green construction applications.

## 2. Results and Discussion

Natural wood contains many lumina (i.e., wood channels) that are aligned through the material in the tree growth direction (Figure 2a). A large number of tubular channels (10–70 μm in diameter) inside the wood structure provide porous structure with sufficient oxygen that harms its fire-retardant behavior (Figure 2b; Figure S2, Supporting Information). To remove such features, we fabricated the densified wood by first partially delignifying the material using NaOH/Na<sub>2</sub>SO<sub>3</sub>.<sup>[19–21]</sup> After chemical treatment, the 3D porous wood structure remains, though the morphology changes from elliptic wood cells to crumpled ones (Figure S3a,b, Supporting Information). The twisting wood channels (Figure S3c,d, Supporting Information) and shrunken cell walls cause the natural wood to become softer and more flexible.<sup>[22]</sup> Subsequent hot pressing,

perpendicular to the wood growth direction produces a densified laminated structure (Figure 2c). Figure 2d shows the top-view scanning electron microscopy (SEM) image of the densified wood, where multiple wood channels have collapsed entirely, resulting in intertwined cell walls without intervening gaps. The fully collapsed cell walls provide a unique microstructure for reducing fire hazards by creating an extremely low oxygen content and high density. Fourier-transform infrared (FTIR) spectra of the natural wood and densified wood samples show that the functional groups of wood assigned to hemicellulose (C=O stretching vibration) and lignin (G-lignin and C=O stretching vibration) are partially removed with a total weight loss of 28.8% as a result of the chemical treatment (Figure 2e; Figure S4, Supporting Information).<sup>[23,24]</sup>

We then characterized the wood samples after burning in a cone calorimeter with an external heat flux of 30 kW m<sup>-2</sup> for 2 min (Figure 2f; Figure S5, Supporting Information). As the densified wood is heated and burned, gases are generated inside the densified wood, which flow outward, resulting in the observed porous structure (Figure 2g). The amorphous char layer coated on densified wood surface is further demonstrated in the corresponding FTIR (Figure 2e) and Raman spectra (Figure S6, Supporting Information). The FTIR characteristic peaks of the densified wood appear to be lost after burning, and meanwhile the D and G peaks at 1354 and 1590 cm<sup>-1</sup> in the Raman spectra confirmed the amorphous carbon on the wood surface.<sup>[25,26]</sup> The char layer on the outside surface can act as a thermal barrier, which effectively protects the interior wood

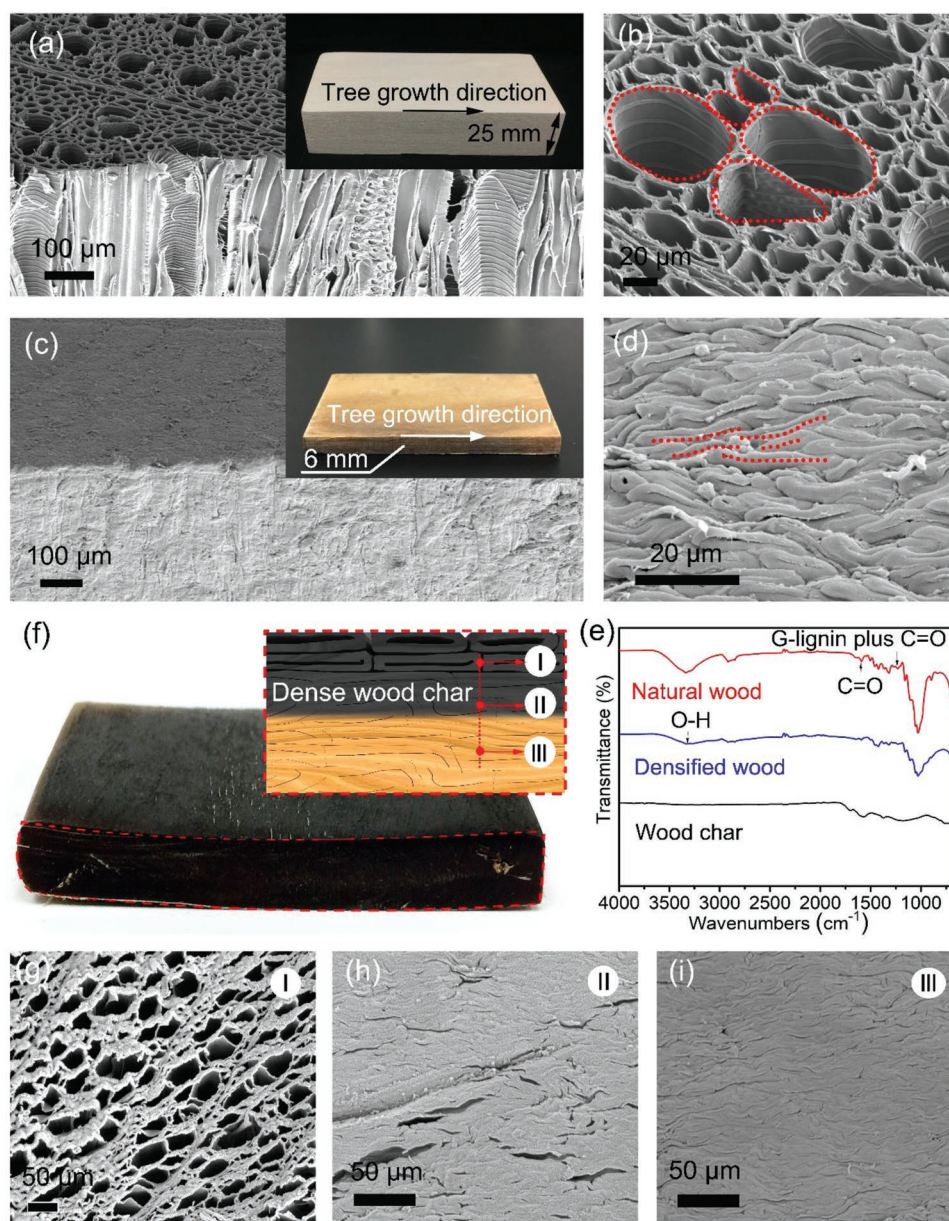


**Figure 2.** Morphology and structural characterization of natural and densified wood. a,b) SEM images of the natural wood: a) cross-sectional view and b) top view. Inset: Photograph of natural wood. c,d) SEM images of the densified wood: c) cross-sectional view and d) top view. Inset: Photograph of the densified wood. e) FTIR spectra of the natural, densified, and wood char samples. f) Photograph of the densified wood after combustion in a cone calorimeter at  $30 \text{ kW m}^{-2}$  for 2 min. g–i) Top-view SEM images of the outside, middle, and inside of the densified wood after combustion. I: The outer layer: porous wood char; II: the middle layer: dense wood char; III: the inner layer: unburned densified wood.

against the rapid increase of temperature, helping to maintain the overall integrity of the densified wood structure.<sup>[27,28]</sup> Meanwhile, a dense char layer underneath the intumescent char layer forms (Figure 2h), which should block most air from transporting into the densified wood and greatly decrease the burning speed. The tightly packed structure of the inner layer should also be important for maintaining the mechanical strength of the wood (Figure 2i). Although the natural wood is also formed a porous char layer during the same burning process, the deformation and cracking have already occurred after exposing at an external heat flux of  $30 \text{ kW m}^{-2}$  for 2 min,

indicating the poor fire retardance of natural wood (Figure S7, Supporting Information).

We qualitatively evaluated the combustion behavior of the natural wood, natural wood after partial delignification, natural wood after hot pressing, and densified wood samples after being exposed directly to an open butane flame. As shown in Figure S8a in the Supporting Information, the natural wood ignited within 5 s, resulting in a significant flame spread. The flammability of natural wood is caused by its components (cellulose, hemicellulose, and lignin) and porous structure. After partial delignification, the treated natural wood shows a similar burning



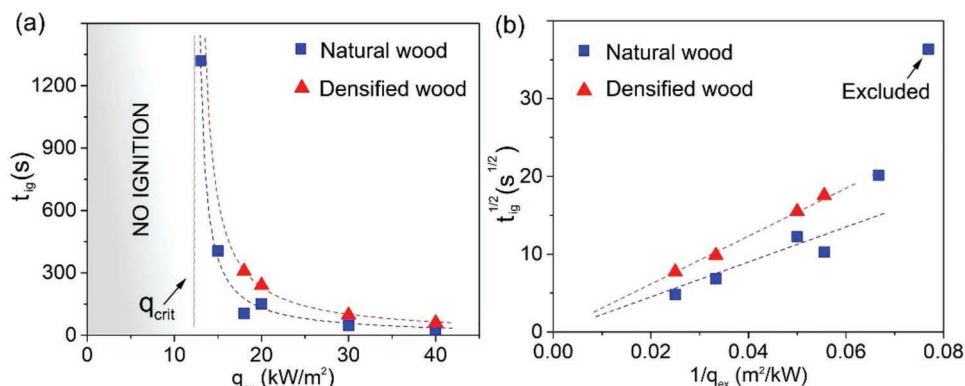


**Figure 3.** Ignition test results from cone calorimeter: data point for  $t_{ig}$  and the fitted  $t_{ig}$  curve plotted with respect to external heat flux values for natural wood and densified wood. a) Critical heat flux ( $q_{crit}$ ) and b) TRP are determined.

behavior as the natural wood but burned out quickly due to the removal of flammable lignin (Figure S8b, Supporting Information). Compared with natural wood and natural wood after delignification, the pressed natural wood without delignification shows slightly delayed ignition and flame spread, revealing the improved fire retardance by the densified wood structure (Figure S8c, Supporting Information). However, the natural wood cannot be completely compressed due to the rigid wood cell walls and the many pores that remain in the pressed natural wood.<sup>[29–31]</sup> By contrast, using our two-step fabrication strategy, the densified wood with a totally collapsed wood structure can withstand continuous exposure to the butane flame until 90 s and self-extinguish at 97 s, clearly demonstrating the structure-induced improvement to the flame resistance (Figure S8d and Videos S1–S4, Supporting Information). In addition, we evaluated the critical heat flux ( $q_{crit}$ ) for ignition as an index parameter for the lowest thermal load needed to initiate a combustion reaction in order to quantitatively characterize the fire retardance of the wood samples.<sup>[32,33]</sup> The cone calorimeter experiment was conducted in accordance with the conditions and equipment specified in ASTM E1354.<sup>[34]</sup> With various external heat fluxes ( $q_{ex}$ ) of 13, 15, 18, 20, 30, and 40 kW m<sup>−2</sup>, the ignition time can be fitted according to Equation (1)<sup>[35,36]</sup>

$$t_{ig} = \frac{b}{q_{ex} - q_{crit}} \quad (1)$$

in which  $b$  is a fitted constant,  $t_{ig}$  is the ignition time,  $q_{ex}$  is the external heat flux, and  $q_{crit}$  is the critical heat flux. As plotted in Figure 3a, the  $t_{ig}$  decreases with increasing  $q_{ex}$  for both wood samples. The fitted curves generally agree with the measurements, with  $R^2$  coefficients of 0.99 for both wood materials, respectively. The corresponding  $q_{crit}$  of both wood samples are 12.2 kW m<sup>−2</sup> since the samples are the same wood material. Ideally for a thermally thick material, the lowest heat flux to introduce ignition compensates the surface heat losses. Ignition temperature is calculated and compared by Equation (2)

$$q_{crit} = h_c (T_{ig} - T_{\infty}) + \sigma (T_{ig}^4 - T_{\infty}^4) \quad (2)$$

where  $h_c$  represents a convective heat transfer coefficient, which is constant to be 15 W m<sup>−2</sup> K<sup>[33]</sup>;  $T_{\infty}$  is the ambient

temperature (298 K), and  $\sigma$  is the Stefan–Boltzmann constant ( $5.67 \times 10^{-8}$  W m<sup>−2</sup> K<sup>−4</sup>). Since the  $q_{crit}$  is the same for both wood sample, the  $T_{ig}$  of wood samples is calculated to be 340 °C (Table 1). Thermal response parameter (TRP) is an indicator of ignition time delay after the materials being exposed to the  $q_{ex}$ . It defines as

$$TRP = \left( \frac{\pi}{4} k \rho c_p \right)^{0.5} (T_{ig} - T_{\infty}) \quad (3)$$

where the product of the thermal conductivity  $k$ , density  $\rho$ , and heat capacity  $c_p$  of the specimen is called the thermal inertia.<sup>[37,38]</sup> The TRP is calculated by Equation (4), which is the slope of the fitted curve in Figure 3b

$$t_{ig} = \left( \frac{TRP}{q_{ex}} \right)^2 \quad (4)$$

Equation (4) is invalid for the  $q_{ex}$  near the  $q_{crit}$ . Thus, the experimental result of  $q_{ex} = 13$  kW m<sup>−2</sup> is excluded from TRP calculation. The higher value of the TRP indicates the longer time to ignition. The TRP of densified wood is  $308 \pm 9$  s<sup>0.5</sup> kW m<sup>−2</sup>, while natural wood only has  $226 \pm 43$  s<sup>0.5</sup> kW m<sup>−2</sup> (Table 1). The thermal inertia of densified wood is  $1.21 \pm 0.21$  s kW<sup>2</sup> m<sup>−4</sup> K<sup>−2</sup>, which is nearly two times higher than natural wood ( $0.657 \pm 0.20$  s kW<sup>2</sup> m<sup>−4</sup> K<sup>−2</sup>). Overall, the densified wood has a lower maximum HRR, average HRR, and heat of combustion ( $\Delta h_c$ ) than natural wood under all the tested  $q_{ex}$ , presenting a better flame retardancy (Table 2).

The material steady burning behavior is further studied. Figure 4a compares the HRR profiles of natural wood and densified wood at an external heat flux of 30 kW m<sup>−2</sup>. The HRR profiles of natural wood and densified wood show two peaks associated with the ignition and maximum heat release rate.

**Table 1.** Measured values of  $q_{crit}$ ,  $T_{ig}$ , TRP, and  $k\rho c_p$  for the testing wood samples. The 95% confidence intervals are shown.

Materials	$q_{crit}$ [kW m <sup>−2</sup> ]	$T_{ig}$ [°C]	TRP [s <sup>0.5</sup> kW m <sup>−2</sup> ]	$k\rho c_p$ [s kW <sup>2</sup> m <sup>−4</sup> K <sup>−2</sup> ]
Natural wood	12.2 ± 0.3	339 ± 4	226 ± 43	0.657 ± 0.20
Densified wood	12.2 ± 2.3	340 ± 34	308 ± 9	1.21 ± 0.21

**Table 2.** Average values of  $HRR_{ave}$ ,  $HRR_{peak}$ ,  $\dot{m}_{ave}$ ,  $t_{burn}$ ,  $\frac{\Delta m}{m_0}$ , and  $\Delta h_c$  for the testing wood samples. The 95% confidence intervals are shown.

Materials	$HRR_{ave}$ [ $\text{kW m}^{-2}$ ]	$HRR_{peak}$ [ $\text{kW m}^{-2}$ ]	$\dot{m}_{ave}$ [ $\text{mg s}^{-1}$ ]	$t_{burn}$ [s]	$\frac{\Delta m}{m_0}$ [%]	$\Delta h_c$ [ $\text{kJ g}^{-1}$ ]
Natural wood	$180 \pm 17$	$259 \pm 22$	$116 \pm 8$	$166 \pm 43$	$50.7 \pm 11$	$14.0 \pm 0.6$
Densified wood	$121 \pm 31$	$194 \pm 12$	$99.8 \pm 30$	$522 \pm 82$	$70.4 \pm 5.5$	$13.0 \pm 2.8$

Figure 4b,c schematically presents the combustion behavior of the natural wood and densified wood, respectively. The incident  $q_{ex}$  pyrolyzes the wood samples by releasing combustible gases. As the mass flow rate of the combustible fuel near the pilot ignitor exceeds the lower flammable limit of the fuel/air ratio, ignition occurs with a rise of HRR to the first peak. As the pyrolysis front grows inward, a layer of char gradually builds up serving as a thermal resistance layer between the wood surface and the inner virgin wood. Therefore, HRR decreases after the first HRR peak. As the temperature grows, the char layer starts to crack on the surface, which creates an easy pathway to the volatiles inside the wood. As the cracks grow wider and deeper, HRR reaches a maximum. We observed that the HRR peaks of the densified wood emerged after longer time and at lower intensities than the natural wood, with a 34.6% reduction in

the maximum HRR peak at an external heat flux of  $30 \text{ kW m}^{-2}$ . Compared with natural wood, the densified wood has a very dense and strong self-formed char layer (Figure S9, Supporting Information), which reduces the flow rate of volatiles and maintains the HRR at a low value for almost 500 s (Figure 4a). As the self-formed char layer starts to crack, the dense structure slows down the growth of these fissures. Thus, the maximum HRR peak of the densified wood is much smaller than that of the natural wood. After the volatiles are exhausted, flaming combustion ceases and smoldering combustion takes place. The reaction then becomes oxidizer diffusion dominated.<sup>[28,34]</sup> The 2.08-fold increase in  $t_{ig}$  and 26% decrease in average HRR of the densified wood further indicates the effectiveness of the dense self-formed char layer in increasing the difficulty of burning the wood (Figure 4d,e). Moreover, we found the effective heat

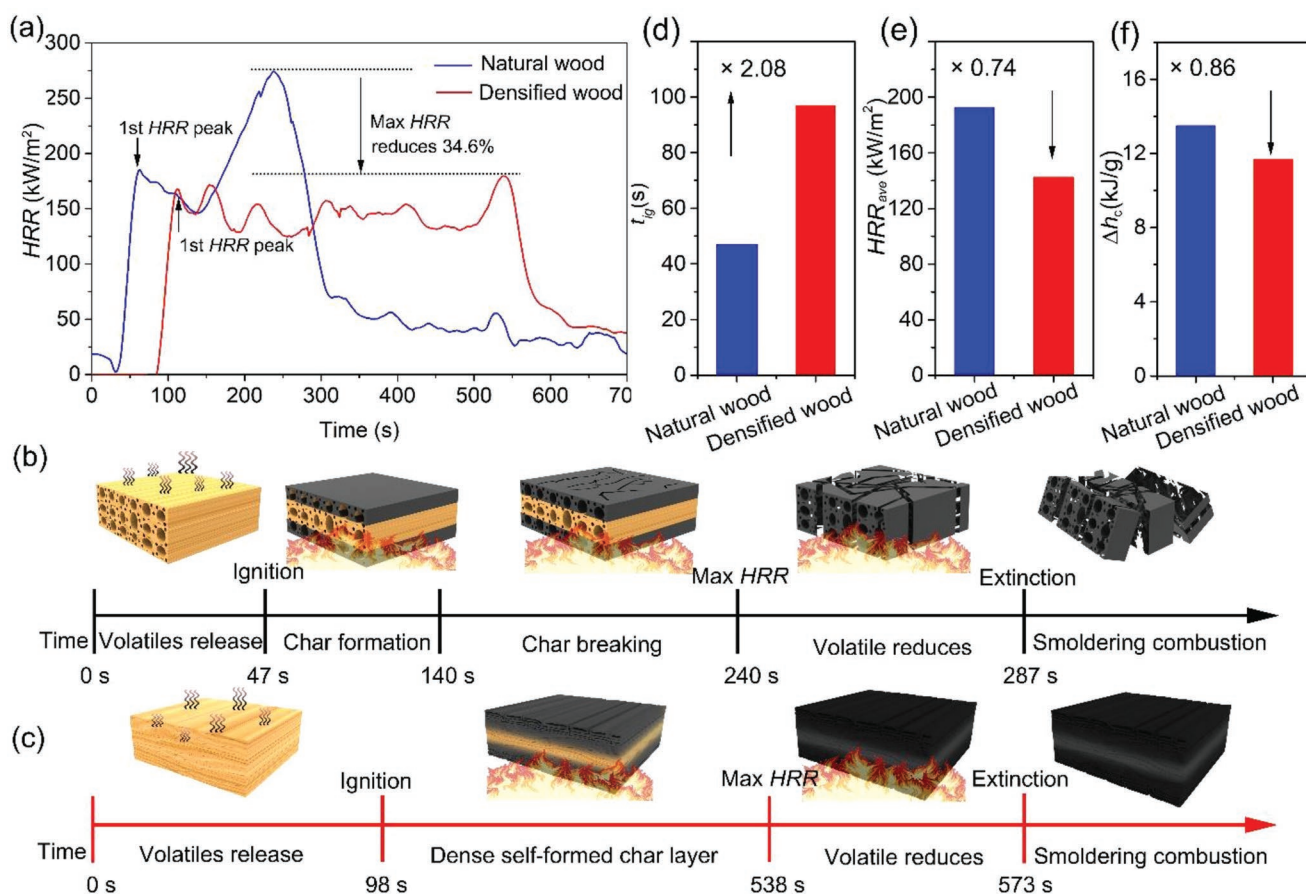


**Figure 4.** a) HRR plots of natural wood and densified wood at an external heat flux of  $30 \text{ kW m}^{-2}$ . Schematic representation of the combustion behaviors of b) natural wood and c) densified wood. d) ignition time, e) average heat release rate, and f) effective heat of combustion of natural wood and densified wood at an external heat flux of  $30 \text{ kW m}^{-2}$ .

of combustion ( $\Delta h_c$ ) of the densified wood decreased by 14% compared with natural wood, indicating the reduction of the heat emission ability of the densified wood during combustion (Figure 4f). Although the total heat release (THR) of the densified wood shows a slightly higher value than that of the natural wood due to its higher density, if divided by mass the specific THR of the densified wood is actually 1.5 times lower (Figures S10 and S11, Supporting Information). Overall, the 2.08-fold increase in  $t_{ig}$ , 34.6% decrease in maximum HRR, 26% decrease in average HRR, and 14% decrease of  $\Delta h_c$  reveal the overall improvement of the fire retardancy of the densified wood. Meanwhile, the steady burning behavior of natural wood and densified wood at the external heat flux of 20 and 40 kW m<sup>-2</sup> are shown in Figures S12 and S13, Supporting Information, respectively. The ignition time for both wood samples decreased as  $q_{ex}$  increased. In general, a higher  $q_{ex}$  pyrolyzes the fuel faster. As a result, the fuel/air gas mixture reaches its lower flammability limit faster and ignition occurs. Table S1 in the Supporting Information lists HRR<sub>ave</sub>, HRR<sub>peak</sub>,  $m_{ave}$ , and  $\Delta h_c$  for both natural wood and densified wood with increasing heat flux. As  $q_{ex}$  increases, the local temperature near the flame increases, which enhances the chemical reaction rates and therefore increases HRR and  $m_{ave}$  for both samples. There is no change in  $\Delta h_c$  with the different values of  $q_{ex}$  since both samples are made of the same wood. However, the obvious improvement in ignition time and the decrease in maximum HRR of densified wood at various heat fluxes confirm the effective fire retardancy of the dense and self-formed char layer on the densified wood surface. The combustion performance between the densified wood without fire retardants and other flame-retardant techniques further proved the superior fire retardancy of densified wood (Table S2, Supporting Information).<sup>[15,16,39–41]</sup>

The rapid decrease in the strength of burned wood caused by the decomposition of its components (cellulose and lignin) is a long-standing challenge in wooden structural design. It is noteworthy that the laminated structure of the densified wood with oriented cellulose nanofibrils contributes to an outstanding mechanical strength,<sup>[29]</sup> which we hypothesized could be maintained even after exposed to fire. We studied the compressive strength of the densified wood after pyrolysis the material in a tube furnace. Figure 5a,d,g shows the schematic representation of the wood compression tests along the growth direction after different burning times at 500 °C in the air. Figure 5b compares the compression stress–strain curves of unburned natural wood and unburned densified wood. Curves of both wood samples show linear deformation behavior before compression failure. The densified wood demonstrates a super high compressive strength of 101 MPa, which is 3.5 times higher than that of natural wood (Figure 5c). With the burning time increased to 60 s, the compressive strength of natural wood was significantly reduced from 39 to 28 MPa, while the compressive strength of the densified wood was maintained at 100 MPa, which is almost the same as its original value (Figure 5e,f). Further extending the burning time to 90 s, the compressive strength of natural wood approached 0 MPa, suggesting the wood material had completely lost its mechanical strength. By contrast, at this burning time the densified wood still maintained a very high compressive strength of 82 MPa, which is still 2.2 times higher

than the unburned natural wood (Figure 5h,i). Figure 5j shows the distinct variations of the compressive strength with heating time for both wood samples. When the heating time increases from 0 to 90 s, the compressive strength loss of the natural wood is 100%, while the densified wood loss is only 18%. The digital images of the wood samples after the compressive tests confirm the significant enhancement in the compressive strength of the densified wood (Figure 5k). The natural wood after burning for 90 s was easily pressed into carbon residue, while the densified wood retained its shape. Moreover, the compressive strength of densified wood along the radius direction (R) and the tangential (T) direction are  $\approx 46$  and 21 times higher than those of natural wood, respectively (Figure S14, Supporting Information). The flexural stress of the densified wood is also about 4.5 and 9.6 times higher than that of natural wood perpendicular to and along the wood growth direction, respectively, indicating the excellent mechanical properties of the densified wood (Figure S15, Supporting Information).

### 3. Conclusion

In conclusion, we have demonstrated an additive-free strategy to simultaneously enhance the mechanical robustness and fire retardancy of wood materials with oriented cellulose nanofibrils by delignification and densification. The laminated structure imparted by the delignification and densification treatment enables the formation of a dense wood char layer on the surface of the densified wood when burned. Consequently, the densified wood displayed a strong increase in thermal response parameter and the time required to reach ignition at a series of external heat flux, indicating a substantial improvement of the ignition degree. Specifically, the densified wood demonstrates an overall enhancement in fire retardancy, including a 34.6% decrease in HRR, a 26% reduction in average HRR, and a 14% decrease of  $\Delta h_c$  at an external flux of 30 kW m<sup>-2</sup>. In addition, the densified wood can be self-extinguished after removing fire. We ascribe the enhanced flame-retardant properties of the densified wood to the self-formed wood char layer, which acts as both a gas barrier and thermal shield that contribute to the delayed thermal degradation of the wood and emission of volatile combustible gases, which greatly protects the interior densified wood structure. Thus, excellent mechanical properties of the densified wood can be well maintained after burning, which greatly improves the fire safety of wood materials. This wood char self-formation mechanism induced by the densified wood structure is demonstrated to be a promising, sustainable, and efficient method for fire protection and reinforcement, which can be used as a stand-alone alternative or in combination with current flame-retardant solutions. The mechanically robust and fire-retardant densified wood offers a practical solution toward safe, durable, and green buildings.

### 4. Experimental Section

**Materials and Chemicals:** Basswood (Saunders Midwest LLC) was used in the study. The chemicals used in this work for partial lignin

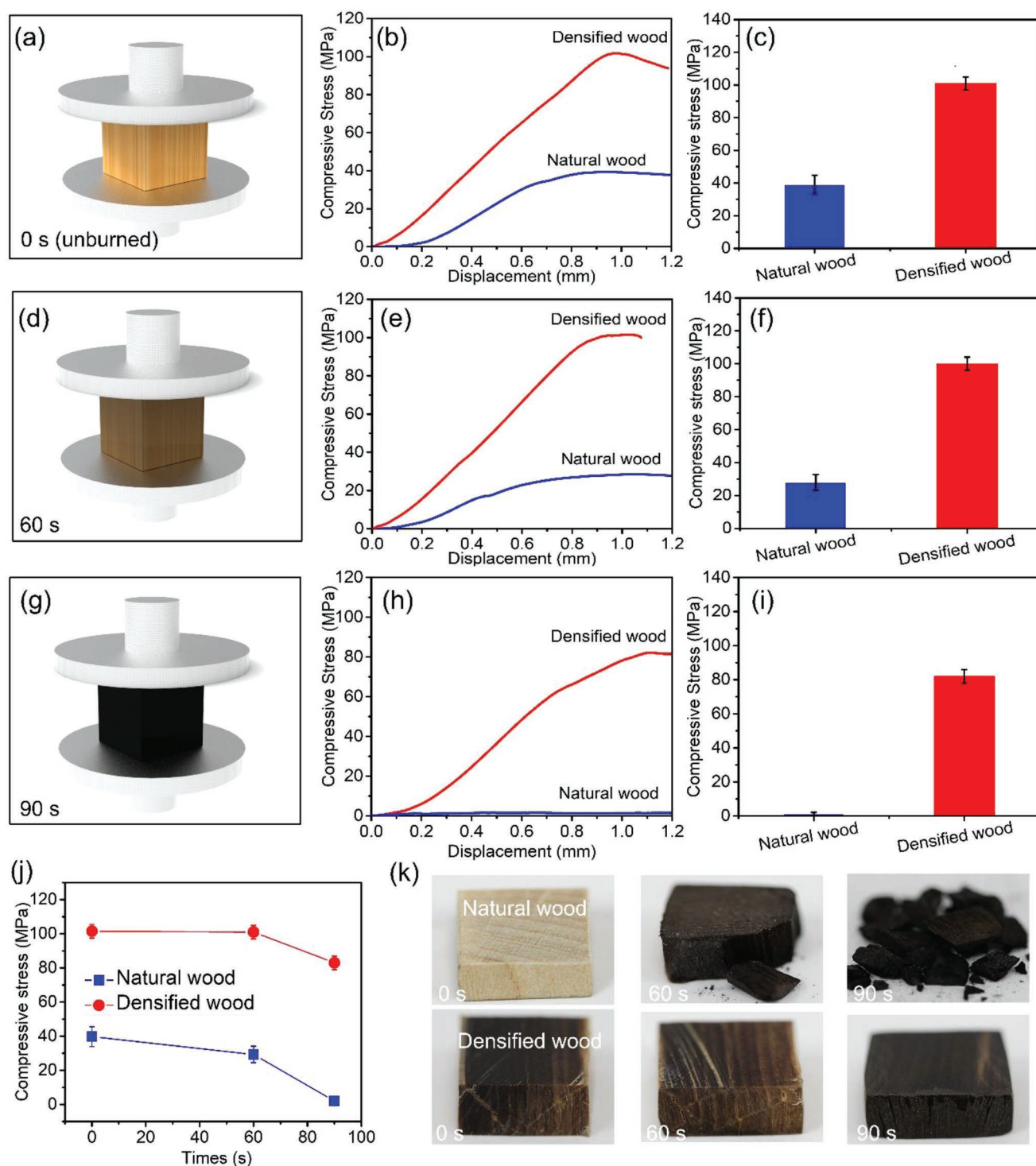


**Figure 5.** Compressive strength of natural wood and densified wood. a,d,g), Schematics of compression tests of the natural and densified wood samples after different burning times. b,e,h), Corresponding compressive stress as a function of compressive displacement of the wood samples. c,f,i), Comparison of the corresponding compressive strengths of the natural and densified wood materials. j) Variation of the compressive strength of the natural and densified wood. k) Photograph of the wood samples after the compressive tests.

removal were  $\text{Na}_2\text{SO}_3$  (>98%, Sigma-Aldrich) and  $\text{NaOH}$  (>98%, Sigma-Aldrich).

**Synthesis:** Natural wood samples (typical wood dimensions: 10 cm × 10 cm × 25 mm; 10 cm × 5 cm × 25 mm) were immersed in 1000 mL

of mixed 2.5 M  $\text{NaOH}$  and 0.4 M  $\text{Na}_2\text{SO}_3$  solution and boiled for 24 h, followed by rinsing in distilled water several times to remove the chemicals. Then, the wood samples were pressed at 100 °C under a pressure of 5 MPa for ≈24 h to obtain the densified wood



(10 cm × 10 cm × 6 mm; 10 cm × 5 cm × 6 mm). The experimental details are shown in Figure S16 in the Supporting Information.

**Characterization:** The morphology of the wood samples was observed by SEM using a Hitachi SU-70 SME. FTIR spectra were recorded on a 6700 spectrometer (USA) over the range of 600–4000 cm<sup>-1</sup> to determine the functional groups of the wood samples. Raman spectra were performed on a LabRAM Aramis model (Horiba Jobin-Yvon) using a 532 nm laser.

**Mechanical Tests:** Wood specimens of 9 mm (tangential) × 9 mm (radial) × 4.5 mm (longitudinal) were first heated in a tube furnace (OTF-1200X) at 500 °C for 0, 60, and 90 s in an air atmosphere. Then, the deformation behavior under compression was measured using a Tinius Olsen H5KT tester with a cross-head speed of 1 mm min<sup>-1</sup>. For three-point bending tests, the dimensions of the wood samples were 50 mm by 50 mm by 7 mm. The span between the two bottom rollers is 34 mm and the top roller pressing down with the speed of 1 mm min<sup>-1</sup>.

**Butane Flame Test:** Wood samples with a size of 20 mm × 20 mm × 7 mm were vertically fixed. A butane flame with 4 cm luminous length was used to ignite the wood sample for 60 s. The angle between the wood and the flame was fixed at 30° to ensure full contact.

**Cone Calorimetry Measurements:** The combustion tests were carried out on a cone calorimeter according to the ASTM E1354.<sup>[34]</sup> Equipment used in accordance with the standard includes a conical radiant electric heater, specimen holders, an exhaust gas system with oxygen monitoring (Servomex 540E) and flow measuring instrumentation (Omega FMA-1680A), an electric ignition spark plug, a data collection (Fluke ITS-90) and analysis system, and a load cell (Satorius WZA8202-N). The incident heat fluxes used were 13, 15, 18, 20, 30, and 40 kW m<sup>-2</sup>.

## Supporting Information

Supporting Information is available from the Wiley Online Library or from the author.

## Acknowledgements

W.G., C.C., and Z.W. contributed equally to this work. L.H., W.G., and C.C. designed the experiments. W.G., C.C., and J.S. contributed to wood processing and mechanical measurements. Z.W., P.B.S., and W.G. contributed to the fire resistance measurements and analysis. W.G. and Y.K. created the 3D illustrations. R.M. and S.H. provided characterizations via SEM and FTIR. L.H., W.G., and C.C. collectively wrote the paper. All authors commented on the final manuscript. The authors acknowledge the support of the Maryland Nanocenter, its Surface Analysis Center and AIMLab. The authors also acknowledge the help from Dr. Glenn Pastel on the Raman tests. W.G. acknowledges the financial support by the China Scholarship Council (CSC).

## Conflict of Interest

The authors declare no conflict of interest.

## Keywords

cellulose nanofibrils, delignification, densification, flame retardance, structural materials

Received: October 22, 2018

Revised: January 5, 2019

Published online: February 15, 2019

- [1] M. J. Karter, *Fire Loss in the United States during 2010*, National Fire Protection Association Quincy, MA 2011.
- [2] T. Li, M. Zhu, Z. Yang, J. Song, J. Dai, Y. Yao, W. Luo, G. Pastel, B. Yang, L. Hu, *Adv. Energy Mater.* **2016**, 6, 1601122.
- [3] G. Wimmers, *Nat. Rev. Mater.* **2017**, 2, 17051.
- [4] M. Zhu, J. Song, T. Li, A. Gong, Y. Wang, J. Qi, Y. Yao, W. Luo, D. Henderson, L. Hu, *Adv. Mater.* **2016**, 28, 5181.
- [5] X. Dong, X. Zhuo, J. Wei, G. Zhang, Y. Li, *ACS Appl. Mater. Interfaces* **2017**, 9, 9070.
- [6] L. A. Berglund, I. Burgert, *Adv. Mater.* **2018**, 30, 1704285.
- [7] I. Watanabe, S.-i. Sakai, *Environ. Int.* **2003**, 29, 665.
- [8] I. Van der Veen, J. de Boer, *Chemosphere* **2012**, 88, 1119.
- [9] L. Dong, C. Hu, L. Song, X. Huang, N. Chen, L. Qu, *Adv. Funct. Mater.* **2016**, 26, 1470.
- [10] Z. L. Yu, N. Yang, V. Apostolopoulou-Kalkavoura, B. Qin, Z. Y. Ma, W. Y. Xing, C. Qiao, L. Bergström, M. Antonietti, S. H. Yu, *Angew. Chem., Int. Ed.* **2018**, 57, 4538.
- [11] A. C. Balazs, T. Emrick, T. P. Russell, *Science* **2006**, 314, 1107.
- [12] K. Liu, W. Liu, Y. Qiu, B. Kong, Y. Sun, Z. Chen, D. Zhuo, D. Lin, Y. Cui, *Sci. Adv.* **2017**, 3, e1601978.
- [13] X. Gao, L. Huang, B. Wang, D. Xu, J. Zhong, Z. Hu, L. Zhang, J. Zhou, *ACS Appl. Mater. Interfaces* **2016**, 8, 35587.
- [14] Z. L. Yu, N. Yang, L. C. Zhou, Z. Y. Ma, Y. B. Zhu, Y. Y. Lu, B. Qin, W. Y. Xing, T. Ma, S. C. Li, *Sci. Adv.* **2018**, 4, eaat7223.
- [15] Q. Fu, L. Medina, Y. Li, F. Carosio, A. Hajian, L. A. Berglund, *ACS Appl. Mater. Interfaces* **2017**, 9, 36154.
- [16] B. Guo, Y. Liu, Q. Zhang, F. Wang, Q. Wang, Y. Liu, J. Li, H. Yu, *ACS Appl. Mater. Interfaces* **2017**, 9, 23039.
- [17] J. Liu, R. G. Kutty, Q. Zheng, V. Eswariah, S. Sreejith, Z. Liu, *Small* **2017**, 13, 1602456.
- [18] N. Wang, Y. Fu, Y. Liu, H. Yu, Y. Liu, *Holzforschung* **2014**, 68, 781.
- [19] Q. Wang, X. Zhao, J. Zhu, *Ind. Eng. Chem. Res.* **2014**, 53, 11007.
- [20] C. Chen, J. Song, S. Zhu, Y. Li, Y. Kuang, J. Wan, D. Kirsch, L. Xu, Y. Wang, T. Gao, Y. Wang, H. Huang, W. Gan, A. Gong, T. Li, J. Xie, L. Hu, *Chem* **2018**, 4, 544.
- [21] J. Guo, K. M. A. Uddin, K. Mihhels, W. Fang, P. i. Laaksonen, J. Zhu, O. J. Rojas, *ACS Sustainable Chem. Eng.* **2017**, 5, 6978.
- [22] J. Song, C. Chen, C. Wang, Y. Kuang, Y. Li, F. Jiang, Y. Li, E. Hitz, Y. Zhang, B. Liu, A. Gong, H. Bian, J. Y. Zhu, J. Zhang, J. Li, L. Hu, *ACS Appl. Mater. Interfaces* **2017**, 9, 23520.
- [23] R. Rana, R. Langenfeld-Heyser, R. Finkeldey, A. Polle, *Wood Sci. Technol.* **2010**, 44, 225.
- [24] N. Gierlinger, L. Goswami, M. Schmidt, I. Burgert, C. Coutand, T. Rogge, M. Schwanninger, *Biomacromolecules* **2008**, 9, 2194.
- [25] C. Chen, Y. Li, J. Song, Z. Yang, Y. Kuang, E. Hitz, C. Jia, A. Gong, F. Jiang, J. Zhu, B. Yang, J. Xie, L. Hu, *Adv. Mater.* **2017**, 29, 1701756.
- [26] Y. Huang, E. Ma, G. Zhao, *Ind. Crops Prod.* **2015**, 69, 447.
- [27] L. Kong, H. Guan, X. Wang, *ACS Sustainable Chem. Eng.* **2018**, 6, 3349.
- [28] S. Ullah, F. Ahmad, A. Shariff, M. Bustam, *Polym. Degrad. Stab.* **2014**, 110, 91.
- [29] J. Song, C. Chen, S. Zhu, M. Zhu, J. Dai, U. Ray, Y. Li, Y. Kuang, Y. Li, N. Quispe, Y. Yao, A. Gong, U. H. Leiste, H. A. Bruck, J. Y. Zhu, A. Vellore, H. Li, M. L. Minus, Z. Jia, A. Martini, T. Li, L. Hu, *Nature* **2018**, 554, 224.
- [30] L. Laine, T. Belt, L. Rautkari, J. Ramsay, C. A. Hill, M. Hughes, *J. Mater. Sci.* **2013**, 48, 8530.
- [31] K. Laine, K. Segerholm, M. Wälinder, L. Rautkari, M. Hughes, *Wood Sci. Technol.* **2016**, 50, 883.
- [32] V. Babrauskas, *J. Fire Prot. Eng.* **2002**, 12, 163.



- [33] L. A. Lowden, T. R. Hull, *Fire Sci. Rev.* **2013**, 2, 4.
- [34] ASTM E1354, *Standard Test Method for Heat and Visible Smoke Release Rates for Materials and Products Using an Oxygen Consumption Calorimeter*, ASTM, West Conshohocken, PA **1999**.
- [35] A. Tewarson, *Generation of Heat and Chemical Compounds in Fires*, SFPE Handbook of Fire Protection Engineering, Quincy, MA **1995**.
- [36] R. H. White, K. Sumathipala, *Proc. Fire Mater. 2013 Conf.*, San Francisco, California, USA **2013**.
- [37] C. Tonelli, M. Grimaudo, *Energy Build.* **2014**, 83, 89.
- [38] S. Verbeke, A. Audenaert, *Renewable Sustainable Energy Rev.* **2017**, 73, 654.
- [39] X. He, X. J. Li, Z. Zhong, Q. Mou, Y. Yan, H. Chen, L. Liu, *Fire Mater.* **2016**, 40, 818.
- [40] M. S. Mahr, T. Hübert, B. Schartel, H. Bahr, M. Sabel, H. Militz, *J. Sol-Gel Sci. Technol.* **2012**, 64, 452.
- [41] V. Merk, M. Chanana, S. Gaan, I. Burgert, *Holzforschung* **2016**, 70, 867.